Tr. J. of Engineering and Environmental Science
23 (1999) , 9 – 18.

Boundary Shear Stress in Rectangular Compound Channels

Issam A. Al-KHATIB
Institute of Community and Public Health,
Birzeit University, West Bank, PALESTİNE
Nabil M. DMADI
Faculty of Engineering, An-Najah National
University, Nablus, West Bank, PALESTİNE

Received 13.11.1996

Abstract

Experimental results are presented concerning the boundary shear stress distribution in a rectangular compound section channel comprising rectangular main channel and two symmetrically disposed floodplains. Different dimensionless ratios of shear stress distributions are obtained and related to relevant parameters. The floodplains due to the momentum transfer between the deep section and floodplains has been investigated. Some important results concerning the uniformity of shear stress distribution which is significant in alluvial channels to state the possible locations of erosion and deposition have been presented.

Key Words: Open channel, compound section, shear stress, alluvial channel

Kompozit Dikdörtgen Kanallarda Duvar Kesme Gerilmesi

Özet

Bileşik diktörtgen kesitli kanallarda ana kanal ve taşma kanallardaki cidar kesme gerilmesi deney sonuçları sunulmuştur. Kesme gerilmesinin ilgili parametrelere dayanan boyutsuz oranları elde edilmiştir. Ana kanal ve taşma kanlallardaki geometrik değişimin, alt kesit ve taşma kanallar arasındaki momentum transferi incelenmiştir. Alüvyonlu kanallarda önemli olan, erozyon ve birikim lokasonları ile ilgili önemli kesme gerilmesi dağılımları sunulmuştur.

Anahtar Sözcükler: Açık kanal, bileşik kesit, kesme gerilmesi, alüvyonlu kanallar.

Introduction

Many flood-routing methods assume a simple cross section for purposes of calculation of the stage-discharge characteristics of rivers. These methods therefore ignore the transform of momentum between the main channel and its floodplains.

Owing to simplistic models, calibration with one set of data does not necessarily ensure reliable results for other data, particularly if for one of the cases the floodplains are inundaed. The reduced hydraulic radius of the floodplain and the often higher hydraulic roughness results in lower velocities on the floodplains than in the main channel. These differences result in a bank of vortices as demonstrated by Knight and Hamid (1984) referred to as "turbulence phenomenon". There is therefore a lateral transfer of momentum that results in apparent shear stress.

Information regarding the nature of boundary shear stress distribution in a flowing stream is needed for various purposes: to give a basic understanding of the resistance relationship, to understand the mechanism of sediment transport, for designing stable channels and for designing revetments and so on for channels where meandering phenomena are predominant (Ghosh and Jena, 1971).

The boundary shear stress distribution and flow resistance in compound cross section channels have been investigated by many authors (Lai, 1986; Lai and Knight, 1988; Myers and Brennan, 1990; Rhodos and Lamb, 1991; Rhodos and Knight, 1994; Knight and Cao, 1994).

The aim of this study was to describe the effect of the interaction mechanism on shear stress distribution in channel of compound cross section. Specially the effect of the main channel width and step height on the variation of shear stress distribution in both main channel and floodplain channel for constant flow discharges was investigated.

Experimental Apparatus

All series of experimets were conducted in a glass-walled horizontal laboratory flume 9.0 m long, 0.67 m wide and 0.75 m deep, at the Hydromechanics Laboratory of the Middle East Technical University.

The volumetric flow rate was measured with a rectangular sharp-crested weir mounted in he inlet box of the flume. Head measurements over the crest for this weir was done by a point gauge of 0.01 cm accuracy and predetermined calibration curve of the weir was used to determine the discharges. The maximum capacity was around 110 lt/sec.

In the course of experiments, for head measurements a point gauge was used along the centreline of flume. All depth measurements were done with respect to the bottom of the flume. A pitot tube of circular section with external diameter of 7 mm was used to measure the static and total pressures which were used for velocities and shear stresses at required points in the experiments conducted throughout this study.

Models of rectangular compound cross sections were manufactured from Plexiglas and placed at about mid length of the laboratory flume. Fig. 1 shows the plan wiew, longitudinal profile and cross section of the models with symbols designating important dimensions of model elements. The dimensions of the various models used in the experiments are given in Table 1. In this study model types tested are denoted by BIZI (I=0, 1, 2, 3). Here B and Z are width and step height of the main channel of the compound cross section, respectively. When I=0, BI and ZI become B0Z0, which means the first type of model which is the laboratory flume, in which there is no compound channel and the bottom slope has a value of 0.005.

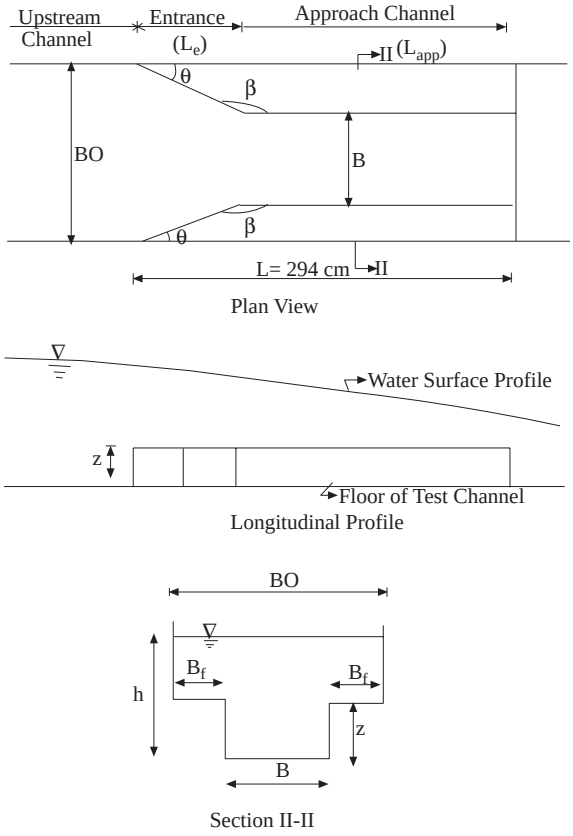

Figure 1. Definition Sketch of the Flume used in the Experiments.

The expeirments first were conducted in the models of smallest B (= 20 cm) with varying Z vlues (=5 cm, 10 cm 15 cm) and then B was increased to 30 cm at the required amount of Z=5 cm, 10 cm, and 15 cm, and finally for B=45 cm with the same three values of Z. All the compound cross section models were constructed on a horizontal bottom slope channel.

Measurement of Wall Shear Stress

Preston (1954) developed a simple technique for measuring local shear on smooth boundaries in a turbullent boundary layer using a pitot tube (or Preston tube) placed in contact with the surface. The

method is based on the assumption of an inner law (law of the wall) which relates the boundary shear stress to the velocity distribution near the wall. Assessment of the near wall velocity distribution is empirically inferred from the differential pressure between pitot tube and static wall pressure tapping. Patel (1965) undertook further experiments to produce a reliable land definitive calibration curve to replace that developed by Preston. Patel's calibration curve which has been shown to be reliable may be summarised as follows (Isaacs and Macintosh 1990).

Table 1. Dimensions and Dimensionless Values of Models

Types of models	B (cm)	Z (cm)	B_f (cm)	B_0 (cm)	θ (degree)	β (degree)	BO/B_f (-)	BO/Z (-)	BO/B (-)	B_f/Z (-)	B_f/B (-)	B/Z (-)
B0Z0	67	-	-	67	-	-	-	-	1	0.00	0.00	-
B1Z1	20	5	23.5	67	26.57	153.43	2.85	13.40	3.35	4.70	1.18	4.00
B1Z2	20	10	23.5	67	26.57	153.43	2.85	6.70	3.35	2.35	1.18	2.00
B1Z3	20	15	23.5	67	26.57	153.43	2.85	4.47	3.35	1.57	1.18	1.33
B2Z1	30	5	18.5	67	26.57	153.43	3.62	13.40	2.23	3.70	0.62	6.00
B2Z2	30	10	18.5	67	26.57	153.43	3.62	6.70	2.23	1.85	0.62	3.00
B2Z3	30	15	18.5	67	26.57	153.43	3.62	4.47	2.23	1.23	0.62	2.00
B3Z1	45	15	11.0	67	26.57	153.43	6.09	13.40	1.49	2.20	0.24	9.00
B3Z2	45	10	11.0	67	26.57	153.43	6.09	6.70	1.49	1.10	0.24	4.50
B3Z3	45	15	11.0	67	26.57	153.43	6.09	4.47	1.49	0.73	0.24	3.00

$$X^* = log_{10}\left[\frac{\Delta P d^2}{4\rho v^2}\right] \quad (1)$$

and

$$Y^* = log_{10}\left[\frac{\tau_0 d^2}{4\rho v^2}\right] \quad (2)$$

where ΔP= Preston tube pressure difference; d= probe outside diameter; ρ= fluid density; ν= kinematic viscosity of the fluid; τ_0 = boundary shear stress; X*= the log of dimensionless differential pressure; Y*= the log of dimensionless shear stress. Patel (1965) produced three equatons covering the range $0.0 < Y^* < 5.3$:

$$Y^* = 0.5X^* + 0.037 \quad (3)$$

$$Y^* = 0.8287 - 0.1381X* + 0.1437X^{*2} - 0.0060X^{*3} \quad (4)$$

$$X^* = Y^* + 2log_{10}(1.95Y^* + 4.10) \quad (5)$$

where: Eq. 3 is applicable for $0.0 < Y^* < 1.5$,
Eq.4 is applicable for $1.5 < Y^* < 3.5$
Eq. 5 is applicable for $3.5 < Y^* < 5.3$

As it is seen, the Preston-tube method to obtain wall shear stress is much more simpler than the Clauser plot which requires detailed velocity measurements.

The technique has been widely used for measurement of boundary shear stresses in both smooth and rough open channels. Recent research utilising the technique includes Knight and Macdonald (1979), Knight (1981), Knight and Demetriou (1984), Baird and Ervine (1984), Knight and Lai (1985) and McKee et al. (1985).

To determine the wall shear stress at the bottom of the main channel and along the floodplain bottom, the measurements were taken by Preston tube at successive points. Upon the analysis of data obtained from experiments considering Eqs. 3-5, the shear stress distributions at the main channel and the floodplain bottom were calculated for each experiment carried out.

Presentation and Discussion of Results

The measured and calculated quantities from the experiments conducted by Al-Khatib (1993) were utilised. In the following section results of the experiments are summarised.

Shear stress patterns were obtained for 11 different depths of flow, each corresponding to a certain discharge. Some of these depths were within the main channel step height only while the others were within the full cross section related to the geometry of each model. The following notations are used in this study:
$\bar{\tau_{mc}}$= average shear stress at the bottom of the main channel; $\bar{\tau_0}$=mean channel shear stress and equals $\rho g R S_e$; g= gravitational acceleration; R=hydraulic radius of the compound channel; S_e= energy slope; $(\tau_{mc})_{max}$= maximum shear stress at the bottom of the main channel; $\bar{\tau}_f$ = average shear stress at the bed of floodplains; $(\tau_f)_{max}$= maximum sher stress at the bed of the floodplains; $\bar{\tau}_{BOZO}$= average shear stress at the bottom of the first model BOZO.

The following subsections give the details of the effect of interaction mechanism on shear stress dis-

tribution in models of different geometry.

Variation of $\bar{\tau}_{mc}$ with Discharge, Q

The relationship between $\bar{\tau}_{mc}$= and Q for some of the models tested are shown in Figs. 2 and 3. The wall shear stress was integrated numerically over the bottom of the main channel and an average value, $\bar{\tau}_{mc}$, was obtained for each set of experiments and plotted against discharge. It can be seen from all the related figures that the average shear stress at the bottom of the main channel increases as discharge increases.

In order to see the effect of the main channel width, B, on the values of $\bar{\tau_{mc}}$ for constant step height, Z, Fig. 2 was plotted. From this figure it is clearly seen that for a given discharge as B increases $\bar{\tau_{mc}}$ increases also. The same trend can easily be noticed in the other models tested (Al-Khatib 1993). Fig. 3 is another form of the data representation for $\bar{\tau_{mc}}$ and Q to investigate the effect of step height, Z, on $\bar{\tau_{mc}}$ as a function of Q for models of constant main channel width. From this figure one can conclude that as the Z values increase in channels of constant main channel with for a given discharge, $\bar{\tau_{mc}}$ values increase.

Variation of $(\tau_{mc})_{max}/\bar{\tau}_0$ with the Relative Depth, Y_r

The experimental results are shown in Figs. 4-7 as $(\tau_{mc})_{max}/\bar{\tau}_0$ versus the relative depth, Y_r, which is the floodplain to main channel water depths ratio, for some of the models tested. The relative depth is directly affected by the geometry of the compound cross section. From these figures it can easily be seen that shear ratios are significantly affected at low depths with irregularities in the pattern and the occurrence of high and low ratios. Since flow in alluvial channels is influenced significantly by shear it is obvious that the previous conclusion will be relevant in the analysis and design of such channels. The increases and decreases in shear stress will indicate regions of possible erosion and scour, while the disturbance of shear ratios will indicate a similar reaction by a channel in erodable material.

In order to see the effect of channel geometry on the $(\tau_{mc})_{max}/\bar{\tau}_0$ versus Y_r the figures were divided into two categories. The first one covers Figs. 4 and 5 and similar figures in which B values were fixed while changing Z values. The figures show that the $(\tau_{mc})_{max}/\bar{\tau}_0$ ratio is mostly irregular for high Z values and reaches its maximum value of 1.6 in the model of B2Z3. On the other hand Fig. 6 and similar figures are plotted to see the effect of varying B values on the $(\tau_{mc})_{max}/\bar{\tau}_0$ ratio versus Y_r for constant Z values. The figures indicate that as B values increase the $(\tau_{mc})_{max}/\bar{\tau}_0$ ratio increases for a given Y_r value and then does not significantly vary with Y_r.

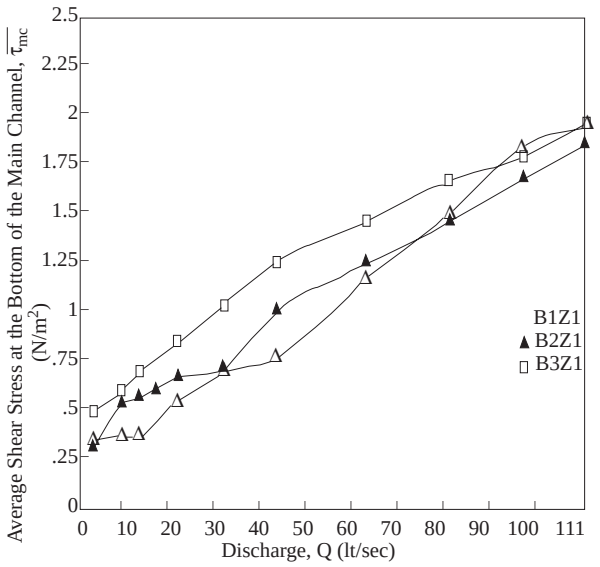

Figure 2. Average Shear Stress at the Bottom of the Main Channel Versus Discharge for models of Constant Step Height, Z1

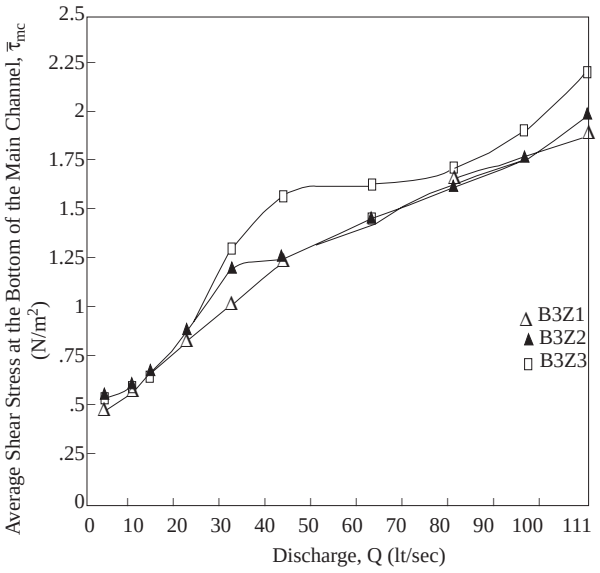

Figure 3. Average Shear Stress at the Bottom of the Main Channel Versus Discharge for models of Constant Step Channel Width, B3.

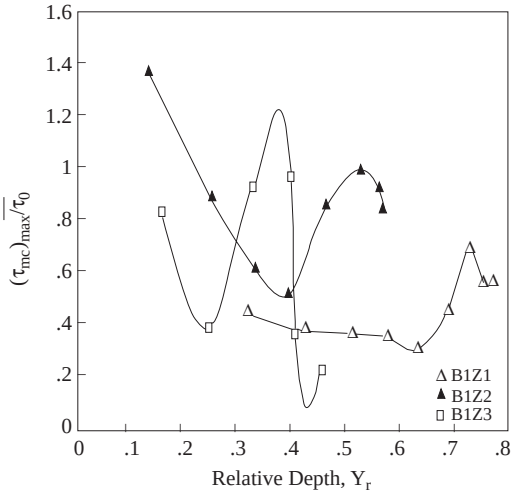

Figure 4. Variation of the Maximum Main Channel Bed Shear Stress to Average Full Cross Sectional Shear Stress Ratio Versus Relative Depth for Models of Constant Main Channel Width, B1.

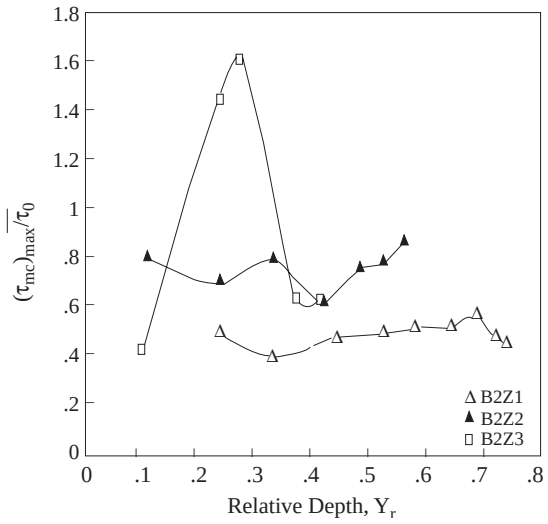

Figure 5. Variation of the Maximum Main Channel Bed Shear Stress to Average Full Cross Sectional Shear Stress Ratio Versus Relative Depth for Models of Constant Main Channel Width, B2.

It will be of significance, however, to compare our results with those of Ghosh and Jena (1971). Their work was carried out in a complex channel consisting of a deep section 204 mm wide by 102 mm deep and two floodplains, each 76 mm wide by 102 mm deep giving a total depth of 204 mm. Of particular interest is a comparison of shear ratios in this complex channel and in moels B1Z1 (I=1, 2, 3) since the width of the main channel in all these models are almost the same. Fig. 7 shows the variation of the ratio of the maximum channel bed shear stress to average full cross sectional shear stress with the relative depth for both the models tested in this study and those of Ghosh and Jena. It can be seen that the difference consists in significantly lower ratios in the present work than those of Ghosh and Jena. It would appear that the explanation of this lies in the differences in channel geometry, in that the B1Z1 models had two floodplains of much larger widths than those used by Ghosh and Jena. The wider floodplains would give rise to lower channel shear, because of loss of energy to the floodplain. This in turn would result in lower ratios for the same cross sectional area of the channel. Thus it is posseble, even on the bases of these few results, to detect a trend depending on channel geometry.

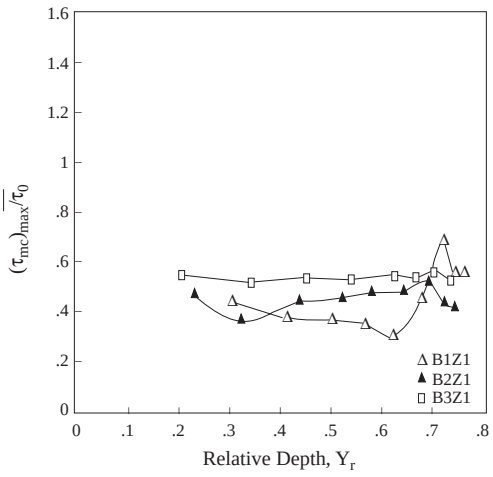

Figure 6. Variation of the Maximum Main Channel Bed Shear Stress to Average Full Cross Sectional Shear Stress Ratio Versus Relative Depth for Models of Constant Step Height, Z1.

Variation of $\bar{\tau_{mc}}/\tau_{B\bar{O}ZO}$ with Q

Figs. 8 and 9 show the variation of $\bar{\tau_{mc}}/\tau_{B\bar{O}ZO}$ with Q for some of the models tested. In order to see the effect of channel geometry on the $\bar{\tau_{mc}}/\tau_{B\bar{O}ZO}$ ratio with Q, the figures are divided into two groups. The first group consists of Fig. 8 and similar figures in which the effect of step height, Z, on the values of $\bar{\tau_{mc}}/\tau_{B\bar{O}ZO}$ for models of constant main channel width are searched for. The $\bar{\tau_{mc}}/\tau_{B\bar{O}ZO}$ ratio increases with increasing Z for a given flow discharge. For three different main channel widths, the step height of Z3 gives the maximum value of $\bar{\tau_{mc}}/\tau_{B\bar{O}ZO}$.

The second group of figures, include Fig. 9 and similar figures, show the effect of varying B values on the $\bar{\tau_{mc}}/\tau_{B\bar{O}ZO}$ ratio with Q for constant Z values. It is clearly seen from Fig. 9 that for a given Q the $\bar{\tau_{mc}}/\tau_{B\bar{O}ZO}$ ratio increases as the B values increase for constant Z. Eventually we can conclude that B3ZI models(I=1, 2, 3) give the maximum $\bar{\tau_{mc}}/\tau_{B\bar{O}ZO}$ ratio for any Q investigated. We can also see from the related figures that the $\bar{\tau_{mc}}/\tau_{B\bar{O}ZO}$ is always less than 1.0. This is because of two reasons. The first reason is that the slope of the first model B0Z0 is equal to 0.005 while the bottom slopes oof the other models are zero. So as the bottom slope of the main chnnel increases, the shear stress at the bottom of the main channel will increase. The second reason is that the first model, B0Z0 has a rectangular cross section while the other models have two symmetrical floodplains. The reduction in the main channel shear stress is due to the presece of the interaction mechanism between the main channel and floodplains. This has the effect of reducing shear values due to the momentum transfer from the main channel to he floodplains. This effect is seen in all the figures related to the compound cross sections, where the $\bar{\tau_{mc}}/\tau_{B\bar{O}ZO}$ ratio is always less than unity.

Variation of $(\tau_f)_{max}/\bar{\tau_0}$ with Floodplain Depth, Y_f

It is known from studies in channels with loose boundaries that a ratio of significant importance is that of maximum shear stress for any element of a cross section to averge cross sectional shear stress. This ratio is an indication of the uniformity of shear distribution and it is significant in alluvial channels to state the possible locations of erosion and deposition. Figs. 10 and 11 show the variation of ratios of maximum floodplain bottom shear stress to average full complex cross sectional shear stress with floodplain depth for constant main channel widths and constant step heights, respectively. From the related figures it can be noticed that $(\tau_f)_{max}/\bar{\tau_0}$ ratio is almost regular for smallest step height Z1 and it becomes irregular for larger step heights. It is quite difficult to say something about the effect of main channel width and step height on the $(\tau_f)_{max}/\bar{\tau_0}$ ratio for a given Y_f value due to the random variation of the data points.

From the above mentioned figures and similar figures it is seen that the interaction between the main channel and floodplains has the effect of decreasing the shear ratios at high depths and also gives rise to significant distubance of the trend at lower depths.

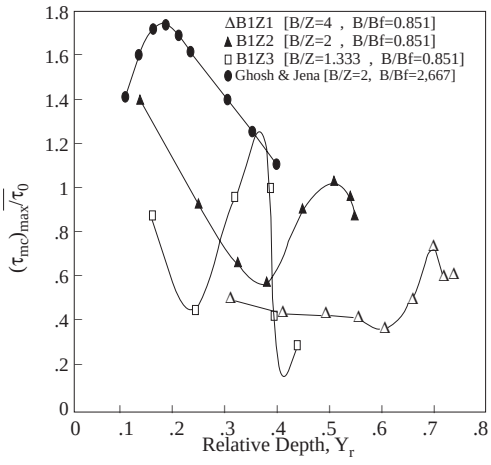

Figure 7. Comparison of Present Results with Those of Ghosh and Jena. Ratio of Maximum Main Channel Bed Shear Stress to Average Full Cross Sectional Shear Stress Versus Relative Depth.

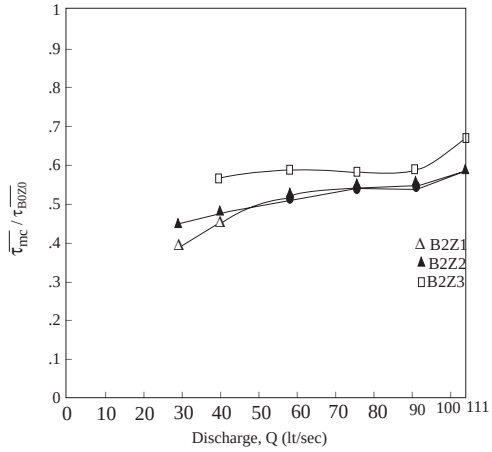

Figure 8. Ratio of the Average Main Channel Bed Shear Stress to Average Bottom Shear Stress of the First Model B0Z0 Versus Discharge for Models of Constant Main Channel Width, B2.

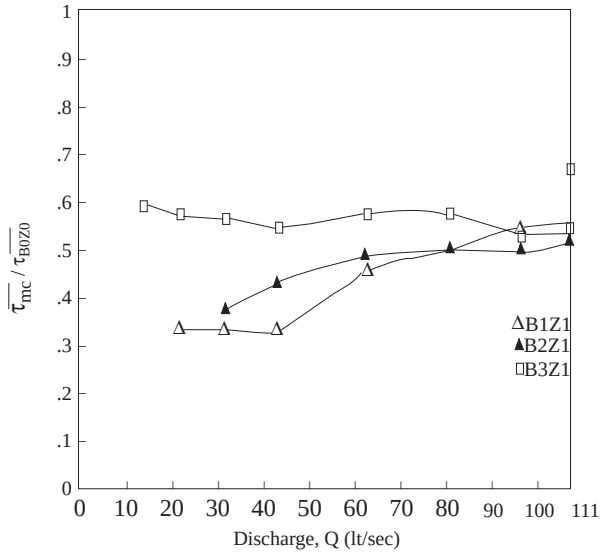

Figure 9. Ratio of the Average Main Channel Bed Shear Stress to Average Bottom Shear Stress of the First Model B0Z0 Versus Discharge for Models of Constant Main Step Height, Z1.

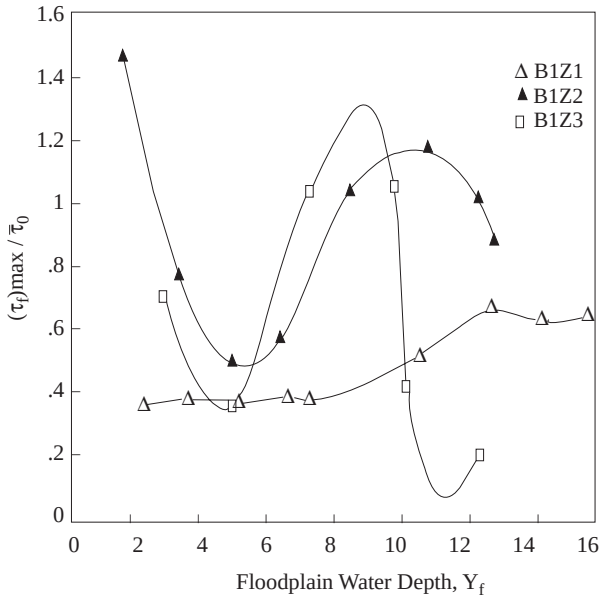

Figure 10. Comparison of Ratios of Maximum Floodplain Bed Shear Stress to Average Full Complex Cross Sectional Shear Stress for Models of Constant Main Channel Width, B1.

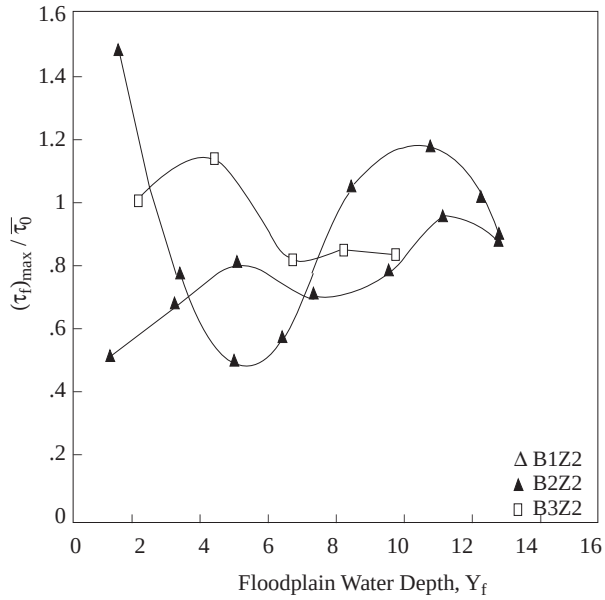

Figure 11. Comparison of Ratios of Maximum Floodplain Bed Shear Stress to Average Full Complex Cross Sectional Shear Stress for Models of Constant Main Step Height, Z2.

It will be of significance, however, to compare the experimental results with those of Myers and Elsawy (1975). Their work was carried out in a complex channel consisting of a deep section 254 mm wide by 101.6 mm deep and one floodplain of 355.6 mm wide by 76.2 mm deep giving a total depth of 177.8 mm. Of particular interest is a comparison of shear ratios of this complex channel and those of models B1ZI (I=1, 2, 3). Fig. 12 shows variations of maximum floodplain bed shear stress to average full cross sectional shear stresss with floodplain depth for both the models used in this study and that of Myers and Elsawy. It can be seen that the difference consists in lower ratios in most of the points in the present work than it that of Myers and Elsawy. It would appear that the explanation of this lies in the difference in channel geometry, in that the present models had two floodplains of much less width than that used by Myers and Elsawy. The wider floodplains will extract larger amount of momentum transfer than that of narrow floodplains.

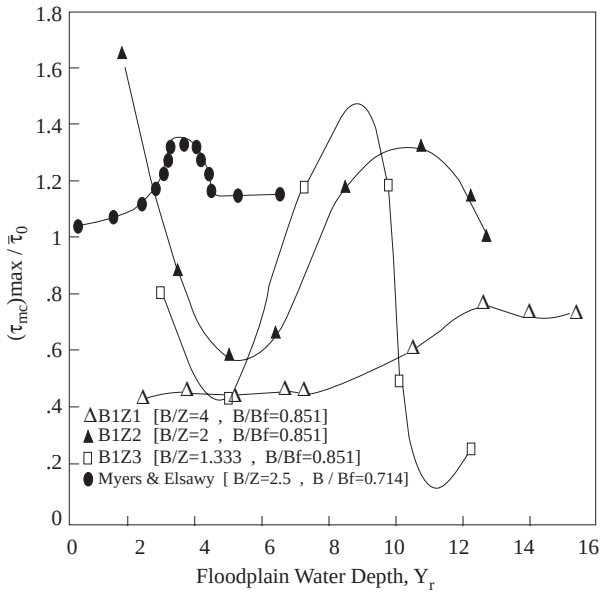

Figure 12. Comparison of Present Results with Those of Myers and Elsawy, 1975. Ratios of Maximum Floodplain Bed Shear Stress to Average Full Complex Cross Sectional Shear Stress.

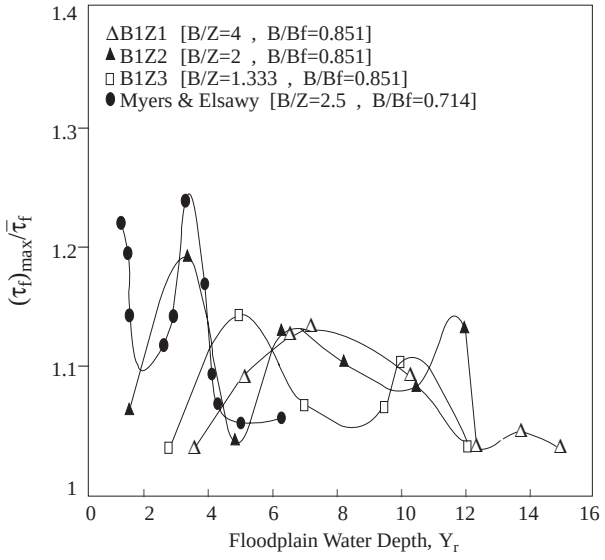

Figure 13. Comparison of Present Results with Those of Myers and Elsawy, 1975. Ratios of Maximum Floodplain Bed Shear Stress to Average Floodplain Shear Stress Versus Floodplain Depth.

Variation of $(\tau_f)_{max}/\bar{\tau}_f$ with Floodplain Depth, Y_f

Wariation of $(\tau_f)_{max}/\bar{\tau}_f$ with floodplain depth Depth, Y_f, is shown in Fig. 13. The wall shear stress was integrated numenrically over the bed of the floodplain, and an average value of the shear stress at the floodplain for each set of data and the ratio of $(\tau_f)_{max}/\bar{\tau_f}$ was calculated and plotted against the floodplain depth. As can be seen from Fig. 13 and similar figures, the presence of interaction introdues irregularities of pattern. Again, a comparison is made between the data of present study and those of Myers and Elsawy mentioned in the previous subsection as it is shown in Fig. 13. The result of comparison is the same as that of the previous subsection. The data of model B1Z2 and those of Myers and Elsawy follow almost the same path since these both models are geometrically very similar to each other, considering B/Z and B/B_f ratios, one can talk about the consistency between experimentally obtained data.

Variation of $\bar{\tau_{mc}}/\bar{\tau_f}$ with Relative Depth, Y_r

Some of the experimental results are shown in Figs. 14 and 15 in the form of $\bar{\tau_{mc}}/\bar{\tau_f}$ versus Y_r. These two figures and similar figures also reveal that the presence of interaction introduces irregularity of pattern. For small Y_r values the shear ratio is greater than unity. But at large Y_r values the ratio approaches to unity or falls a little bit below unity. The reason is that for small Y_r values we have large momentum transfer from the main channel to the floodplains, but at high Y_r values the momentum transfer is in the opposite direction. In order to see the effect of B and Z values on the $\bar{\tau_{mc}}/\bar{\tau_f}$ ratio the figures were divided into two groups. In the first one the main channel width, B, was fixed and the step height, Z, was changed (Fig. 14 and similar figures). Even though it is not possible to give a general conclusion about the variation of $\bar{\tau_{mc}}/\bar{\tau_f}$ for the whole range of Y_r tested, in general one can say that $\bar{\tau_{mc}}/\bar{\tau_f}$ ratio increases as Z values increases. The figures of the second group (Fig. 15 and similar figures) present the data of models of constant step heights. Due to random distribution of data points it is very difficult to say something about the main channel width on the variation of $\bar{\tau_{mc}}/\bar{\tau_f}$ ratio for a given value of Y_r. Finally it can be stated that for a wide range of Y_r the value of $\bar{\tau_{mc}}/\bar{\tau_f}$ ratio varies around unity.

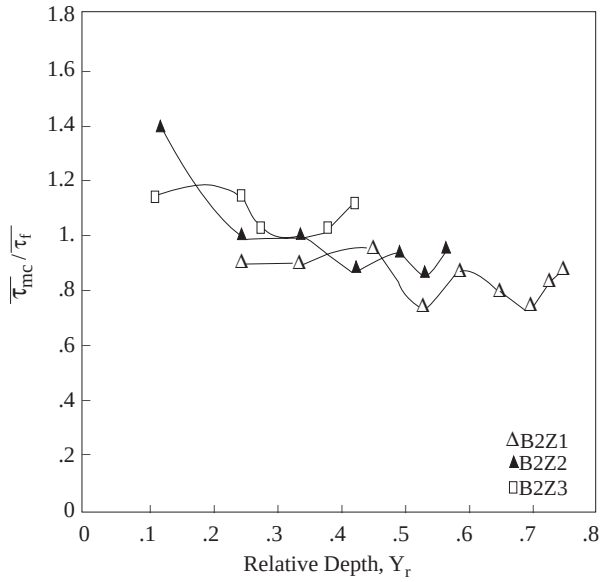

Figure 14. Variation of Ratio of Average Main Channel Bed Shear Stress to Average Floodplain Bed Shear Stress with Relative Depth for Models of Constant Main Channel Width, B2.

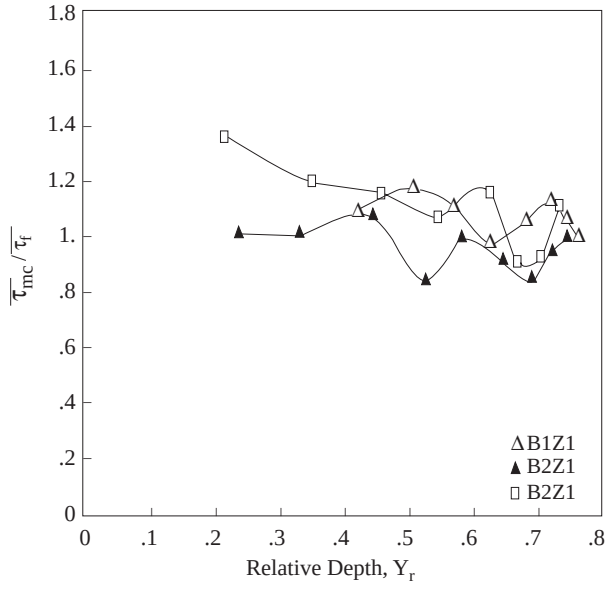

Figure 15. Variation of Ratio of Average Main Channel Bed Shear Stress to Average Floodplain Bed Shear Stress with Relative Depth for Models of Constant Step Height, Z1.

Conclusions

A series of laboratory experiments have been conducted in a smmetrical rectangular compound cross section channel to investigate the geometry effect on the shear stress distirbution in the main channel and floodplains due to the momentum transfer between the deep section and floodplains. From the analysis of the experimental results the following conclusions can be drawn:

1. For a given discharge, in models of constant step height as B increases, τ_{mc}^{-} values increase, and in channels of constant main channel width, if Z values increase, τ_{mc}^{-} values increase.

2. The $(\tau_{mc})_{max}/\bar{\tau}_0$ ratio is mostly irregular for high Z values and reaches its maximum values of 1.6 in the model of B2Z3.

3. As the B values increase the $(\tau_{mc})_{max}/\bar{\tau}_0$ ratio increases for a given Y_r value and then does not significantly vary with Y_r for constant Z values.

4. $\bar{\tau}_{mc}/\bar{\tau}_{BOZO}$ ratio increases with increasing Z for a given discharge. Among three different main channel widths, the step height Z3 gives the maximum value of $\bar{\tau}_{mc}/\bar{\tau}_{BOZO}$.

5.For a given Q, $\bar{\tau}_{mc}/\bar{\tau}_{BOZO}$ ratio increases as B values increase for constant Z. Eventually B3ZI models (I=1, 2, 3) give the maximum $\bar{\tau}_{mc}/\bar{\tau}_{BOZO}$ ratio for any Q investigated.

6. Variation of $(\tau_f)_{max}/\bar{\tau}_0$ ratio with Y_f is an indication of uniformity of shear stress distribution and is important in sediment trasportation. $(\tau_f)_{max}/\bar{\tau}_0$ ratio is almost regular for smallest step height Z1 and it becomes irregular for larger step heights.

7. The general trend of the $(\tau_f)_{max}/\bar{\tau_f}$ versus Y_r curve given by Myers and Elsawy, and the one of model B1Z2 are quite similar due to proper B/Z and B/B_f values.

8. For small Y_r values the $\tau_{mc}^{-}/\bar{\tau_f}$ ratio approaches to unity. The reason is that for small Y_r values we have large momentum transfer from the main channel to the floodplains. For a wide range of Y_r the value the $\tau_{mc}^{-}/\bar{\tau_f}$ ratio varies around unity.

Notation

The following symbols are used in this paper:

B	=	bottom width of the approach channel;
BO	=	bottom width of the upstream channel;
g	=	gravitational accaleration;
d	=	probe outside diameter;

Q	=	volume rate of flow;
R	=	hydraulic radius of the compound channel;
S_e	=	energy slope;
X*	=	the log of dimensionless differential pressure;
Y_f	=	floodplain water depth;
Y_{mc}	=	main channel water depth;
Y_r	=	relative depth which equals the Y_f/Y_{mc} ratio;
Y*	=	the log of dimensionless shear stress;
Z	=	step height;
ρ	=	fluid density;
Δ P	=	Preston tube pressure difference;
v	=	kinematic viscosity of the fluid;
τ_0	=	boundary shear stress;
$\bar{\tau_{mc}}$	=	average shear stress at the bottom of the main channel;
$\bar{\tau_0}$	=	mean channel shear stress and equals ρgRS$_e$;
$(\tau_{mc})_{max}$	=	maximum shear stress at the bottom of the main channel;
$\bar{\tau_f}$	=	average shear stress at the bed of floodplains;
$(\tau_f)_{max}$	=	maximum shear stress at the bed of the floodplains;
$\tau_{B\bar{O}ZO}$	=	average shear stress at the bottom of the first model B0Z0.

References

Al-Khatib, I.A. "Hydraulic characteristics and optimium design of symmmetrical compound channels for flow measurements". Ph.D. thesis, Middle East Tech. Univ., Ankara, Turkey, 1993.

Baird, J.I., and Ervine, D.A., "Resistance to flow in channels with overbank floodplain flow", Proceedings of the 1st International Conference on Channels and Control Structures, 1984.

Ghosh, S., and Jena, S.B., "Boundary shear stress distriubtion in open channel compound". Proceedings of the Institute of Civil Engineers, 49: 417-430, 1971.

Isaacs, L.T., and Macintosh, J.C., "Measurement of shear stress in open channels". Conf. on Hydraulics in Civ. Engrg., The Institution of Engineers, Sydney, Australia, 115-119, 1990.

Knight, D.W., (1981) "Boundary shear in smooth and rough channels. J.Hydr. Div., ASCE, 107(7): 839-851, 1981.

Knight, D.W., and Cao, S. "Boundary shear in the vicinity of river banks". Proc. Nat. Conf. Hydraulic Engrg., ASCE, Buffalo, USA, 1994.

Knight, D.W., and Demetriou, J.D., "Floodplain and main channel flow interaction". J.Hydr. Engrg., ASCE, 109 (8): 1037-1092, 1983.

Knight, D.W., and Hamid, M.E., "Boundary shear in symmetrical compound channels". J. Hydr. Engrg., ASCE, 109 (10): 1412-1427, 1984.

Knight, D.W., and Macdonald, J.A., "Hydraulic resisance of artificial strip roughness". J. Hydr. Div., ASCE,105 (6): 675-690, 1979.

Lai, C.J. "Flow resistance, discharge capacity and momentum transfer in smooth compound closed ducts". Ph.D. Thesis, University of Birmingham, U.K, 1986.

Lai C.J., and Knight, D.W., "distributions of streamwise velocity and boundary shear stress in compound ducts". Proc. 3rd Int. Symp. on Refined Flow Modelling and Turbulence Measurements, IAHR, Ed. Iwasa, Y., Tamai, N. and Wada, A., Tokyo, Japan, 1988.

McKee P.M., Elsawy E.M., and McKeogh E.J., (A study of the hydraulic characteristics of open channels with flodplains". IAHR, Proceedings of the 21 st Congress, Melbourme, Vol. 3, 1985.

Myers, W.R.C. and Brennan, E.K., "Flow resistance in compound channels" J. Hydr. Research, IAHR, 28(2): 141-155, 1990.

Myers, W.R.C., and Elsawy, E.M., "Boundary shear in channels with floodplain" J. Hydr. Div., Vol. 101, No.HY7, pp. 993-1025, 1975.

Patel, V.C., "Calibration of the Preston tube and limitations on its use in pressure gradients". J. Fluid Mech. 23(1): 185-208, 1965.

Preston, J.H., "The determination of turbulent skin friction by means of pitot tubes". J. Royal Aeronautic Society". 58: 109-121, 1954.

Rhodes, D.G., Lamb, E.J., Chance, R.J., and Jones, B.S., "Automatic measurement of boundary shear stress and velocity distributions in duct flow". J. Hydr. Research, IAHR, 29(2): 189-197, 1991.

Rhodes, D.G., and Knight, D.W., "Distribution of shear force on the boundary of a smooth rectangular duct". J. Hydr. Engrg., ASCE 120(7): 787-807, 1994.